



Antimicrobial hydroxyapatite and its composites for the repair of infected femoral condyle

Xinggui Tian^{a,b,c,1}, Zhihui Lu^{a,1}, Chuying Ma^d, Min Wu^a, Chengfei Zhang^e, Yuping Yuan^f, Xiaowei Yuan^g, Denghui Xie^{a,*}, Chao Liu^{d,*}, Jinshan Guo^{a,*}

^a Department of Histology and Embryology, School of Basic Medical Sciences, Guangdong Provincial Key Laboratory of Bone and Joint Degeneration Diseases, The Third Affiliated Hospital of Southern Medical University, Southern Medical University, Guangzhou, China

^b Department of Orthopedics, The Affiliated Hospital of Southwest Medical University Luzhou, Sichuan 646000, PR China

^c University Hospital for Orthopedics and Accident Surgery (OUC), Carl Gustav Carus Dresden University Hospital, TU Dresden, Institute of Public Law of the Free State of Saxony, Fetscherstrasse 74, 01307, Dresden, Germany

^d Aleo BME, Inc., 200 Innovation Blvd, Suite 210A, State College, PA 16803, USA

^e Department of Dentistry, The University of Hong Kong, Hong Kong, China

^f Department of Material Science and Engineering, Southern University of Science and Technology, Shenzhen 518055, China

^g Department of Orthopedics, Shengjing Hospital of China Medical University, Shenyang 110004, China

ARTICLE INFO

Keywords:

Tannin
Silver
Polyurethane
Antimicrobial
Bone regeneration

ABSTRACT

Orthopedic implant-associated infection constitutes one of the most devastating and challenging symptoms in the clinic. Implants without antimicrobial properties may become the harbourage for microbial colonization and biofilm formation, thus hindering normal bone regeneration processes. We had previously developed tannin modified HA (THA) as well as silver and tannin modified hydroxyapatite (HA) (Ag-THA) via a facile one-step and scalable process, and proven their antimicrobial performance *in vitro*. Herein, by compositing with non-antimicrobial polyurethane (PU), the *in vivo* anti-bacterial activity, osteoconductivity and osteoinductivity of PU/Ag-THA composite were investigated using an infected femoral condyle defect model on rat. PU/Ag-THA exhibited excellent *in vivo* antimicrobial activity, with the calculated bacteria fraction being reduced to lower than 3% at week 12 post operation. Meanwhile, PU/Ag-THA is also promising for bone regeneration under the bacteria challenge, evidenced by a final bone mineral density (BMD) ~0.6 times higher than that of the blank control at week 12. A continuous increase in BMD over time was observed in the PU/Ag-THA group, but not in the blank control and its non- or weak-antimicrobial counterparts (PU/HA and PU/THA), in which the growth rate of BMD declined after 8 weeks of operation. The enhanced osteoinductivity of PU/Ag-THA relative to blank control, PU/HA and PU/THA was also confirmed by the Runx2-related transcription factor 2 (RUNX2) and osteocalcin (OCN) immunohistochemical staining. The above findings suggest that antimicrobial Ag-THA may serve as a promising and easy-to-produce antimicrobial mineral for the development of antimicrobial orthopedic composite implants to address the challenges in orthopedic surgeries, especially where infection may become a challenging condition to treat.

1. Introduction

With more than 2.2 million procedures performed worldwide annually, bone transplantation ranks as the second most common tissue transplantation following blood transfusion [1–7]. However, clinical trauma leads to the decrease of blood supply and depression of immune responses, which can cause tissue necrosis and favor microbial invasion

during bone transplantation [8]. Orthopedic implant infection, mostly caused by Gram-positive cocci such as *Staphylococcus aureus*, may occur via the bloodstream, through open wounds (fractures, ulcers, and osteomyelitis) or from surgical procedures, especially when foreign material is implanted. Device or material implantation triggers foreign body response (including acute and chronic inflammation, granulation tissue formation and fibrous encapsulation), and leads to microbial

* Corresponding authors.

E-mail addresses: smuspine@163.com (D. Xie), ch.liu@aleobme.com (C. Liu), jsguo4127@smu.edu.cn (J. Guo).

¹ These authors contributed equally to this work.

colonization and implant infection [9]. In fact, postoperative infections and poor osteogenesis are believed to be the two major causes for orthopedic failure. To address the infection problem, antibiotic impregnated allograft bone [8] and antibiotic-loaded polyacrylate bone cements or other biomaterials [10–12] have been applied in the clinic. As long as the local antibiotic levels are higher than the dosage required for eliminating biofilm embedding, bacteria-derived infections may be inhibited or alleviated. However, the efficacy of loading antibiotics into bone implants is greatly limited and the long-term exposure to low doses of antibiotics is strongly related to the emerging threat of antibiotic resistance in clinics [10]. The development of new antimicrobial strategies in biomaterial design against bone implant infection is in great demand [13].

Chemical or textural surface modification with anti-fouling polymers [13], surface coating with antimicrobial silver nanoparticles or antibiotics [13–15], surface nanotopologic design [13], drug delivery strategy [12,13], and the development of polymeric or inorganic materials with innate antimicrobial properties [16–24] are the commonly used antimicrobial biomaterial design strategies against bone implant infection. Among antimicrobial biomaterials, inorganic and metal antibacterial materials have attracted more and more attention due to their heat resistance, long durability, broad antibacterial spectrum, safe to use and nearly no drug resistance [21–24]. Various metals and their ions, including silver, copper and zinc, exhibit favourable antimicrobial properties, with silver as the strongest and the most widely used agent in orthopedic implant coating due to its broad-spectrum efficiency against bacteria, fungi and even virus [21–25]. It is generally believed that silver ions play a bactericidal role by damaging cell membrane/wall, hindering the electronic and material transmission system, destroying protein (attach to sulfhydryl groups of proteins), inhibiting DNA replication, and producing excessive reactive oxygen species (ROS) [21]. Silver ions or nanoparticles (NPs) can be directly coated on orthopedic implants through processes such as galvanic deposition [25,26], or incorporated into biodegradable polymers [15,17,27].

The catechol or gallotannin (tannin) species employed by mussel- or tannin-inspired adhesion strategies not only can reduce silver ions into

silver NPs, but also can strongly immobilize the *in situ* formed silver NPs into/onto organic and inorganic networks/surfaces through the formation of covalent bonds, hydrogen bonding and/or catechol/gallol-metal complexes [14,15,17,27–29]. Previously, we had developed silver nitrate (SN) crosslinked injectable citrate-based mussel-inspired bioadhesives (iCMBAs) [15] and tannin-inspired gelatin bioadhesives [17] with *in situ* formed silver NPs, which exhibited favourable antimicrobial activity against both bacteria and fungi *in vitro*. Tannin itself is also known to exhibit considerable antimicrobial activity [17]. Tannin-mediated silver NP-coated hydroxyapatite (HA) (silver and tannin modified HA, Ag-THA, Fig. 1A) had also been synthesized through a facile and scalable one-step reaction. Ag-THA was then composited with a citrate-based biodegradable polymer [4,6,30–32], poly(octamethylene citrate) (POC) to form citrate-based tannin-bridged bone composites (CTBCs) that showed considerable antimicrobial properties *in vitro* too [14]. However, the *in vivo* performance of Ag-THA for infection control and for tissue regeneration has not been demonstrated yet.

To further investigate the *in vivo* antimicrobial performance of Ag-THA and to address the challenging problems in regenerating infected bone defects, in this paper, Ag-THA was composited with a representative degradable polymer, alternating block polyurethane (Alt-PU, Fig. 1B) due to its excellent mechanical properties, degradability and biocompatibility for tissue engineering [33–35], to fabricate porous antimicrobial PU/Ag-THA microparticles (MPs) (PU/Ag-THA MPs). The anti-infective, osteoconductive and osteoinductive performance of PU/Ag-THA MPs were assessed in an infected femoral condyle defect models on rats by microcomputed tomography (micro-CT), hematoxylin and eosin (H & E), Masson's trichrome, and Safranin O & fast green staining, as well as Runt-related transcription factor 2 (RUNX2) and osteocalcin (OCN) immunohistochemical staining.

2. Experimental section

2.1. Materials

Hydroxyapatite (HA), tannic acid (TA), silver nitrate (AgNO_3), and

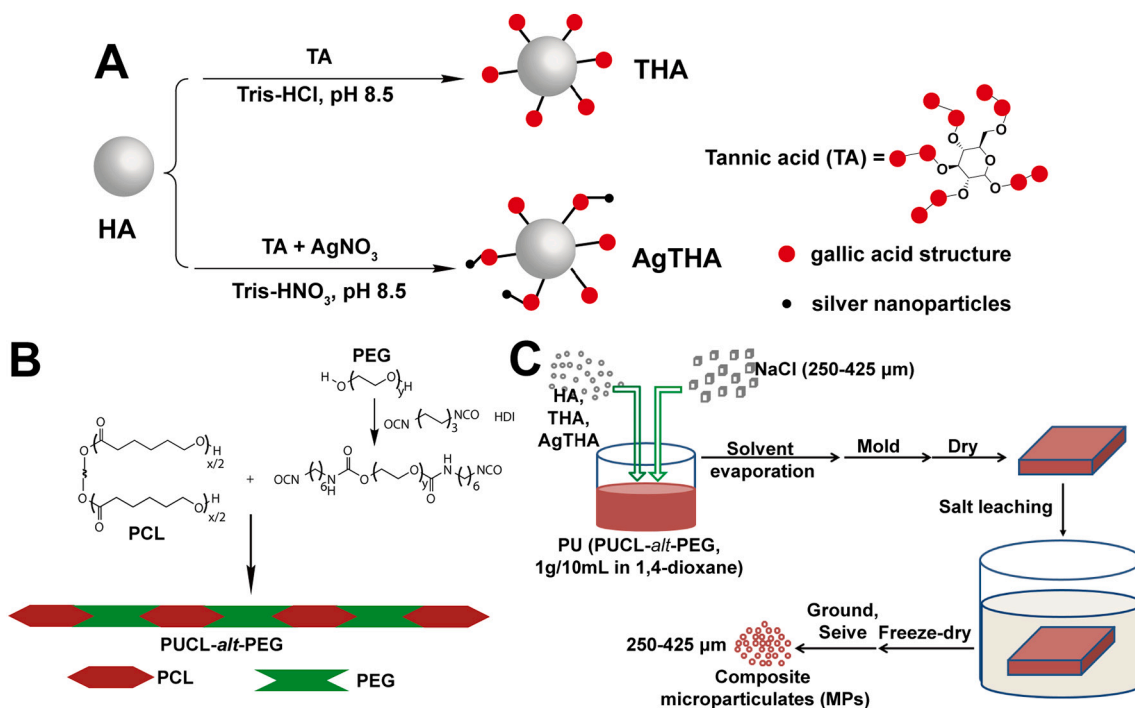


Fig. 1. (A) Synthesis of tannic acid (TA) modified hydroxyapatite (HA) (THA), silver and TA modified HA (AgTHA); (B) synthesis of Alternating block polyurethane (Alt-PU) from poly(ϵ -caprolactone) (PCL) and poly(ethylene glycol) (PEG) (PUCL-alt-PEG); (C) fabrication process of PU/HA, PU/THA and PU/AgTHA composite microparticles (MPs).

other chemicals were all purchased from Sigma-Aldrich and used without further purification.

2.2. Synthesis of TA modified HA (THA) and silver & TA modified HA (Ag-THA)

THA and Ag-THA were synthesized as described in our previous work (Fig. 1A) [14]. For THA synthesis, briefly, 20 g HA dispersing in 150 mL of Tris-HCl buffer (pH 8.5) was reacted with 5 g TA in 50 mL pH 8.5 Tris-HCl buffer solution at room temperature for 24 h. Then the crude product was purified by washing with deionized water and centrifugation for three times to remove salt and unreacted TA, followed by freeze-drying. The synthesis process of Ag-THA was similar with that of THA, but Tris-HCl buffer (pH 8.5) was replaced by Tris-HNO₃ (pH 8.5) buffer (otherwise silver chloride precipitate will form), and for 20 g HA and 5 g TA (in 200 mL pH 8.5 Tris-HNO₃ buffer), 0.5 g AgNO₃ (in 15 mL pH 8.5 Tris-HNO₃ buffer) was added.

2.3. Synthesis of alternating block polyurethane (Alt-PU)

Alt-PU based on poly(ϵ -caprolactone) (PCL) and poly(ethylene glycol) (PEG) (PUCL-alt-PEG) was synthesized according to previous literature [33–35]. Briefly, PEG diol was first reacted with 2-fold 1, 6-hexamethylene diisocyanate (HDI) to obtain PEG-diisocyanate prepolymer in anhydrous 1, 2-dichloroethane, then it was further reacted with PCL diol under nitrogen atmosphere to give PUCL-alt-PEG (Fig. 1B).

2.4. Composite microparticulates (MPs) fabrication

The porous PU/HA, PU/THA and PU/Ag-THA scaffolds (porosity: 80%, pore size: 250–425 μ m) in a cuboid shape (50 \times 50 \times 2 mm) were fabricated using salt leaching method [2,4]. Briefly, 8.0 g sieved sodium chloride (NaCl) crystals (250–425 μ m, as a porogen), 1.0 g Alt-PU (in 10 mL *N,N*-dimethylformamide (DMF)) and 1.0 g HA, THA or Ag-THA (50 wt% of the total weight of HA or modified HA and dry polymer) were mixed and stirred, and fitted into a cuboid Teflon mold (50 \times 50 \times 2 mm). The solvent was evaporated at 50 °C under vacuum for 2 days. The scaffold was soaked in deionized water until the salt was all removed. Then the scaffold was freeze-dried, grounded and sieved to collect the microparticulates (MPs) with sizes between 250 and 425 μ m (Fig. 1C) [4], which were sterilized by ethylene oxide for the following animal study.

2.5. In vivo repair of infected bone defect

Male Sprague-Dawley (SD) rats (8 weeks, 220–250 g, purchased from the Experimental Animal Center of Southern Medical University, Guangzhou, China) were used for the following animal experiments. All surgical procedures as well as perioperative handling were conducted in accordance with protocols approved by the Ethics Committee at the Southern Medical University.

2.5.1. Creation of critical-sized infected femoral condyle defect model on rats and PU/Ag-THA microparticulates (MPs) implantation

Sixty SD rats were randomly assigned to PU/HA, PU/THA, PU/Ag-THA, autograft bone (AB) and blank control (CON) groups, with 12 SD rats in each group. Anesthesia of SD rats was performed by the intraperitoneal injection of 100 mg/kg chloral hydrate. A 1.5–2 cm length incision parallel to the long axis of the femoral shaft was created on the lateral condyle of the femur, which was located using the patellar ligament as the reference. Then the skin and the subcutaneous tissue were cut, to fully expose the lateral condyle of the femur. A 5 mm deep (determined by Vernier caliper) bone defect was drilled in the lateral condyle of the femur using an electric drill with 3.5 mm diameter (critical-sized: Φ 3.5 mm \times 5 mm). To prevent osteonecrosis caused by over-heating, sterile saline was continually dripped during the drilling process. After that, a gauze ball containing 100 μ L *Staphylococcus aureus*

(*S. aureus*, 1×10^6 colony forming units (CFUs)/mL) was implanted into each bone defect, which was then sealed using bone wax (Fig. 2A). 10 days later, pus accumulation and acute periosteal reaction can be found in the defect section, and a large number of bacteria surrounded by a small amount of fibrous tissue can be observed in the H & E and Masson's trichrome staining images (Fig. 2B), indicating the successful creation of infected femoral condyle defect model on rats. PU/HA, PU/THA and PU/Ag-THA composite MPs were then implanted into the infected bone defects after removing bone wax and gauze ball, and thoroughly cleaning the defect sites with sterile saline. A negative control sample was also set with the infected bone defect being left untreated after cleaning.

2.5.2. Microcomputed tomography (micro-CT) analysis

At week 4, 8, and 12 post operation, SD rats were euthanized, the collected femoral condyle specimens (6 for each sample) were harvested, fixed in 4% paraformaldehyde and stored at 4 °C for micro-CT and histology study. Micro-CT (Aloka Latheta LCT-200, Hitachi-Aloka Medical, Ltd., Japan) was conducted in an isolated bone mode to evaluate the bone regeneration in the defect area with the following settings: pixel size, 480 μ m; slice thickness, 240 μ m; slice pitch, 240 μ m; speed, integ. 2; rotation angle, 360°; X-ray voltage, low; artifact removal, lean; sync. scan, no; metal artifact reduction, no. The horizontal and vertical two-dimensional (2D) images of the regenerated femoral condyle sections were reconstructed using VGStudio MAX software (version 2.2.2). A cylindrical space representing the volume of interest (VOI) was designated to evaluate new bone formation by calculating bone mineral density (BMD) using Latheta software (Hitachi Aloka Medical Ltd., Japan). The results are shown in Fig. 3A (horizontal and vertical) and Fig. 4 (enlarged vertical).

2.5.3. Histological study

The fixed specimens were decalcified in 10% ethylenediamine tetraacetic acid (EDTA, pH 7.4) for 30–60 days at 37 °C, followed by alcohol gradient dehydration, dimethyl benzene substitution and paraffin embedding. The embedded specimens were sliced into 4 μ m-thick histological sections and stained with H & E (Fig. 5A), Masson's trichrome (Fig. 5B) and Safranin O & fast green (Fig. 5C) to evaluate the bone regeneration and bacterial infection situation. RUNX2 (Fig. 6A) and OCN (Fig. 6B) immunohistochemical staining were also conducted to assess osteogenesis in the defect area. The stained tissue sections were observed and photographed under bright field microscope (Axio Scope A1, Carl Zeiss Microscopy GmbH, Jena, Germany). The bacteria fractions in different samples at different time points were also calculated by the area percentages from H & E and Masson's trichrome staining images (at least 6 images were used for each sample and the results were averaged) using Image J, and presented in Fig. 5C and D respectively. Numbers of RUNX2 or OCN positive cells per millimeter of bone perimeter were also calculated from the RUNX2 and OCN stained images using Image J, cells were counted from at least six different areas from more than three tissue sections, and the results are shown in Fig. 6C and D respectively.

2.6. Statistical analysis

Data were analyzed using SPSS statistics 20 statistical software (SPSS, Inc., Chicago, IL, USA). All quantitative results are expressed as mean \pm standard deviation. The statistical significance between two sets of data was determined by one-way analysis of variance (ANOVA). Data were taken to be significant if $p < 0.05$ (*) was obtained.

3. Results and discussion

3.1. Design of antimicrobial composite microparticulates (MPs)

In our previous work [14], the *in vitro* antimicrobial activity of Ag-

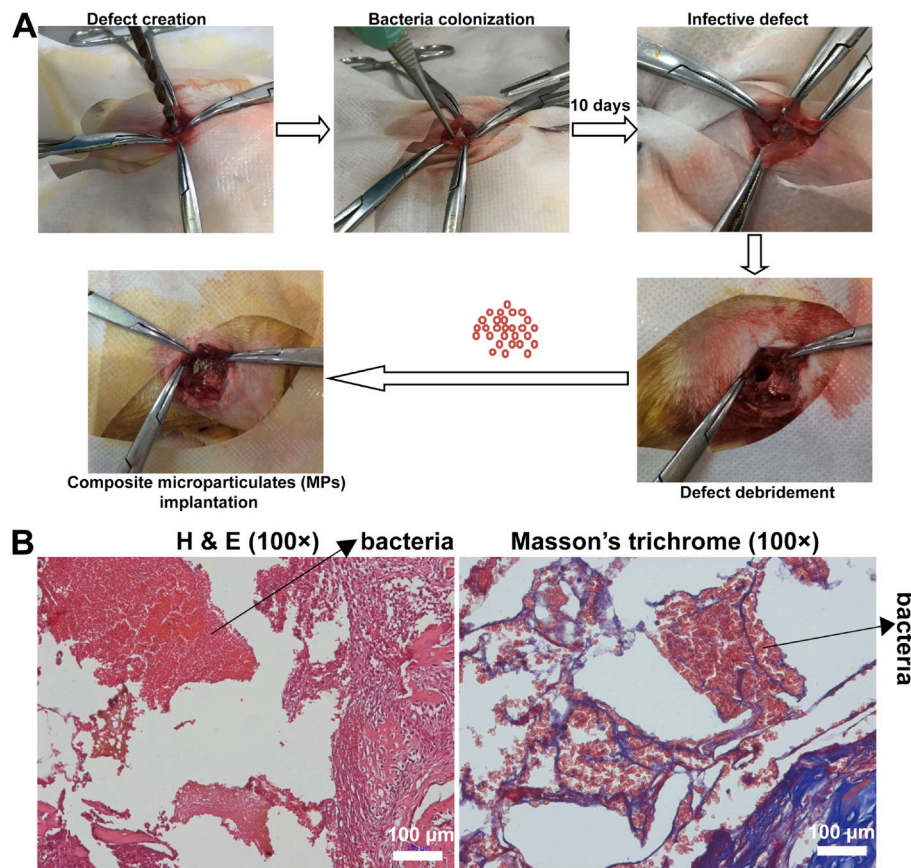


Fig. 2. (A) The creation of infective femoral condyle defects of and their treatment with PU/HA, PU/THA and PU/AgTHA composite microparticulates (MPs); (B) representative H & E and Masson's trichrome staining images of the infected bone defect section.

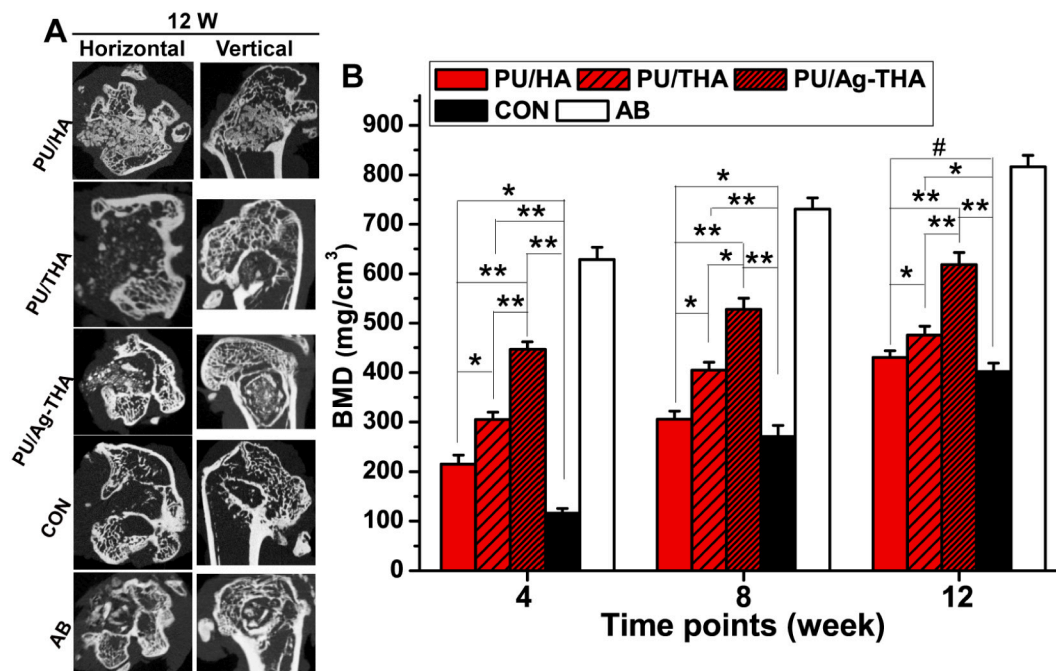


Fig. 3. (A) The representative reconstructed horizontal and vertical 2D micro-CT images of the treated infected femoral condyle defects at week 12 post surgery. (B) The bone mineral densities (BMDs) of infective femoral condyle defects of different groups at week 4, 8 and 12 post surgery (CON: no implantation in the defect; AB: autograft bone). # $p > 0.05$, * $p < 0.05$, ** $p < 0.01$.

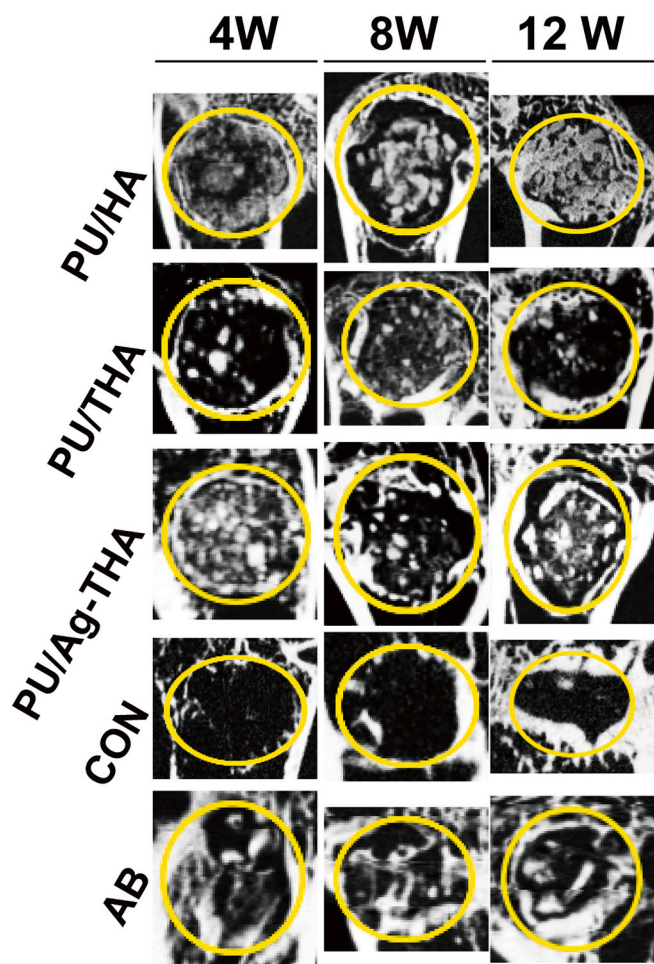


Fig. 4. The enlarged vertical 2D micro-CT images of the treated infected femoral condyle defects 4, 8 and 12 weeks after surgery.

THA and its composites with POC (named CTBCs) against *S. aureus* and *Escherichia coli* (*E. coli*) have been evaluated (e.g., via the minimal inhibitory concentration (MIC) test and bacteria contact-killing activity test). However, the *in vivo* safety and efficacy of Ag-THA in combating the infections while supporting bone growth have yet to be demonstrated. Moreover, the previously developed citrate-based biodegradable polymer [18] also presents inherent antimicrobial properties contributing to the anti-infection activity of CTBCs. Therefore, whether the introduction of Ag-THA could serve as a universal strategy to endow various biomedical polymers with satisfactory antimicrobial properties in a scenario of infected bone regeneration remains elusive. Herein, polyurethane (PU), with well-recorded biocompatibility, flexural endurance, high strength, high wear/abrasion resistance properties, was chosen as the representative polymer to construct antimicrobial composites. Comparing to conventional poly(lactic acid) (PLA) or PCL based hydrophobic polyurethanes, as well as random block polyurethanes (Ran-PU)s made from PLA/PCL and PEG (PULA-ran-PEG [35] or PUL-ran-PEG [34]), alternating block polyurethanes (Alt-PU)s with PLA/PCL and PEG blocks alternately distributing in the polymer chain (PULA-alt-PEG [35] or PUL-alt-PEG [34]), possessed higher crystal degrees, higher mechanical properties, enhanced hydrophilicity, and better wound healing efficiency (exemplified in nerve regeneration) [33–35]. Thus, in this paper, elastic PUL-alt-PEG (Fig. 1B) was applied to composite with Ag-THA to fabricate composite microparticulates (MPs) as shown in Fig. 1C [2,4], and used for bone regeneration in an infected femoral condyle defect model on rats.

3.2. Creation of infected femoral condyle defect and composite MPs implantation

The infected femoral condyle defect model on rats was created by exposing the femoral condyle defect to *S. aureus* for 10 days (Fig. 2A). Successful bacteria colonization and biofilm formation were confirmed by the observation of concentrated bacterial cells in H & E and Masson's trichrome staining images as shown in Fig. 2B [8,36]. PU/HA, PU/THA and PU/Ag-THA composite MPs were then implanted into the infected bone defect sites to evaluate the *in vivo* antimicrobial performance of Ag-THA and its composites with PU. After the operation, the surgical incisions of all rats healed well, there were no obvious postoperative complications such as redness and swelling, and no abnormal activities of all rats were observed.

3.3. Micro-computed tomography (micro-CT) analysis

At the pre-set time points, the infected femoral condyle specimens treated by PU/HA, PU/THA and PU/Ag-THA composite MPs were collected and the micro-CT analysis was conducted. From the reconstructed micro-CT 2D images (Fig. 3A), it can be seen that 12 weeks after surgery, although showing less mineral filling than that of the autograft bone (AB) group, PU/HA, PU/THA and PU/Ag-THA groups showed much more mineral filling than that of the control (CON). This can be confirmed by the enlarged vertical images shown in Fig. 4 (images of week 4 and 8 were also included). In the three composite MP groups, the bone defect was filled with the implanted composites and new bone tissues. The degradation of the composites and gradual new bone tissue formation extended from the defect edge towards the centre were observed (Figs. 3A and 4).

As shown in the quantitative BMD results (Fig. 3B), although the BMDs of the PU/HA, PU/THA and PU/Ag-THA groups at all three tested time points were lower than that of the AB group, they were all significantly higher than that of the CON group except for the PU/HA group at week 12. The BMDs of PU/Ag-THA group at all the three time points were significantly higher than that of PU/HA and PU/THA groups (Fig. 3B). Interestingly, the increase of the BMDs in PU/HA and PU/THA groups seems slower than that of the CON group. Specifically, there was no significant difference between PU/HA and CON groups at week 12, and the difference between PU/THA and CON groups also became much smaller at week 12 (Fig. 3B). This implies that the non-/weak-antimicrobial foreign material may serve as a scaffold for bacteria adherence and survival, and impede the further new bone ingrowth [8]. In contrast, the new bone in the PU/Ag-THA group kept growing after week 8, with a BMD value significantly higher than that of the other two composite MP groups as well as the CON group (Fig. 3B). These results indicate the substantial benefit of the antimicrobial property of Ag-THA in infected bone regeneration compared with its non- or weak-antimicrobial counterparts.

3.4. Histological study

To further investigate the *in vivo* antimicrobial, osteoconductive and osteoinductive performance, histological examination of the decalcified bone tissue sections collected at the pre-set time points was conducted including H & E, Masson's trichrome, and Safranin O/fast green staining, as well as RUNX2 and OCN immunohistochemical staining.

It is conspicuous that plenty of bacteria colonies could be observed from both H & E and Masson's trichrome staining images (Fig. 5A and B), which were wrapped by fibrous tissue. The number of bacteria gradually decreased along with the in-growth of new bone and fibrous tissue, probably because that the newly formed bone can recruit immune cells to the infection sites through blood supply, to alleviate the bone infection to some extent. It was also confirmed by the bacteria (area) fractions calculated from the H & E and Masson's trichrome staining images using Image J (Fig. 5D and E). Specifically, the bacteria fraction

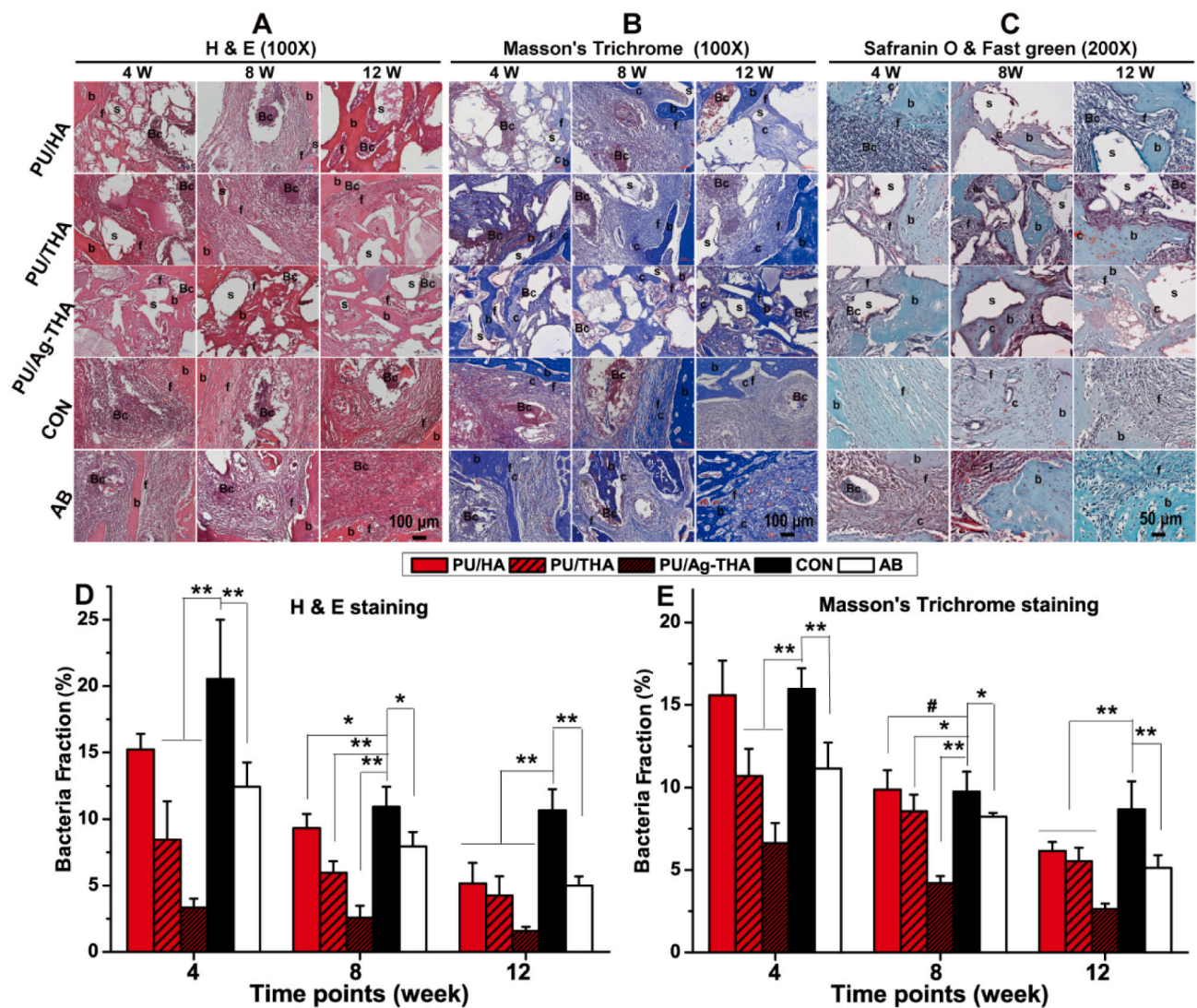


Fig. 5. Representative H & E (hematoxylin and eosin, A), Masson’s trichrome (B) and Safranin O & fast green (C) staining images of the infective bone defect of femoral condyle sections for PU/HA, PU/THA, PU/AgTHA, blank control (CON) and AB groups 4, 8 and 12 weeks after operation; the bacteria fractions in different samples at different time points, which were calculated using Image J based on the H & E (D) and Masson’s trichrome (E) staining images respectively. b: bone, c: cartilage, f: fibrous tissue, s: scaffold, Bc: bacteria. #*p* > 0.05, **p* < 0.05, ***p* < 0.01.

of the CON group was the largest in the beginning, and gradually decreased over time with a significant number of bacteria left evidently observed even after 12 weeks. The bacteria fractions of the AB group were much smaller than that of the CON group, which might be attributed to the inclusion of healthy autograft bone (from other sites) that helped reduce bacteria infection. However, after 12 weeks, a large number of bacteria still survived in the AB group (Fig. 5A, B, D and E), implying that the immune system of the animals is not sufficient to eliminate all the bacteria. Started from the similar level, the bacteria fractions in PU/HA group became larger than that of the AB group at week 12 (Fig. 5A, B, D and E), indicating that the implantation of non-antimicrobial foreign biomaterial into infected bone defect might even favor bacterial adherence, survival and colonization, consistent with the micro-CT analysis. PU/THA exhibited certain “weak” antimicrobial activity, which can be confirmed by the smaller bacteria fractions at week 4 (Fig. 5D and E), compared with that of the PU/HA group. However, the bacteria fractions of the PU/THA group became comparable to that of the PU/HA group at week 8 and 12, suggesting the short duration of the antimicrobial activity of PU/THA or THA. Of note, the bacteria fractions of PU/Ag-THA group were the smallest in all tested composite groups, which were decreased to lower than 3% after 12 weeks. They were also

significantly lower than that of the CON and AB groups at all time-points (Fig. 5D and E). Consistently, the most robust antimicrobial performance of PU/Ag-THA composite MPs was also confirmed by the Safranin O & fast green staining images displaying a markedly reduced bacteria fraction in the PU/Ag-THA group (Fig. 5C). These results together revealed the *in vivo* long-lasting antimicrobial activity of Ag-THA, probably due to the outstanding bacteria killing property of silver ions or silver NPs [34]. Meanwhile, the introduction of TA bearing multiple phenol groups to bridge HA and silver NPs further added benefit to ensure the long-lasting and stable releasing of Ag, which is highly desired for combating bone infection that often recurs for several times post-surgery.

Both H & E and Masson’s trichrome staining (Fig. 5A and B) show new bone and fibrous tissue in-growth into the infected bone defect for PU/HA, PU/THA and PU/Ag-THA groups. It indicated that all three composite MPs could obviously provide support to induce *de novo* trabecular bone formation, which was consistent with the micro-CT analysis. In the AB group, more bone tissue could be found at week 12 (Fig. 5A and B) compared with other groups, confirming the favourable bone regenerative effects of autograft bone as the gold standard, even in infected bone defects. In the CON group, even after 12 weeks, the defect

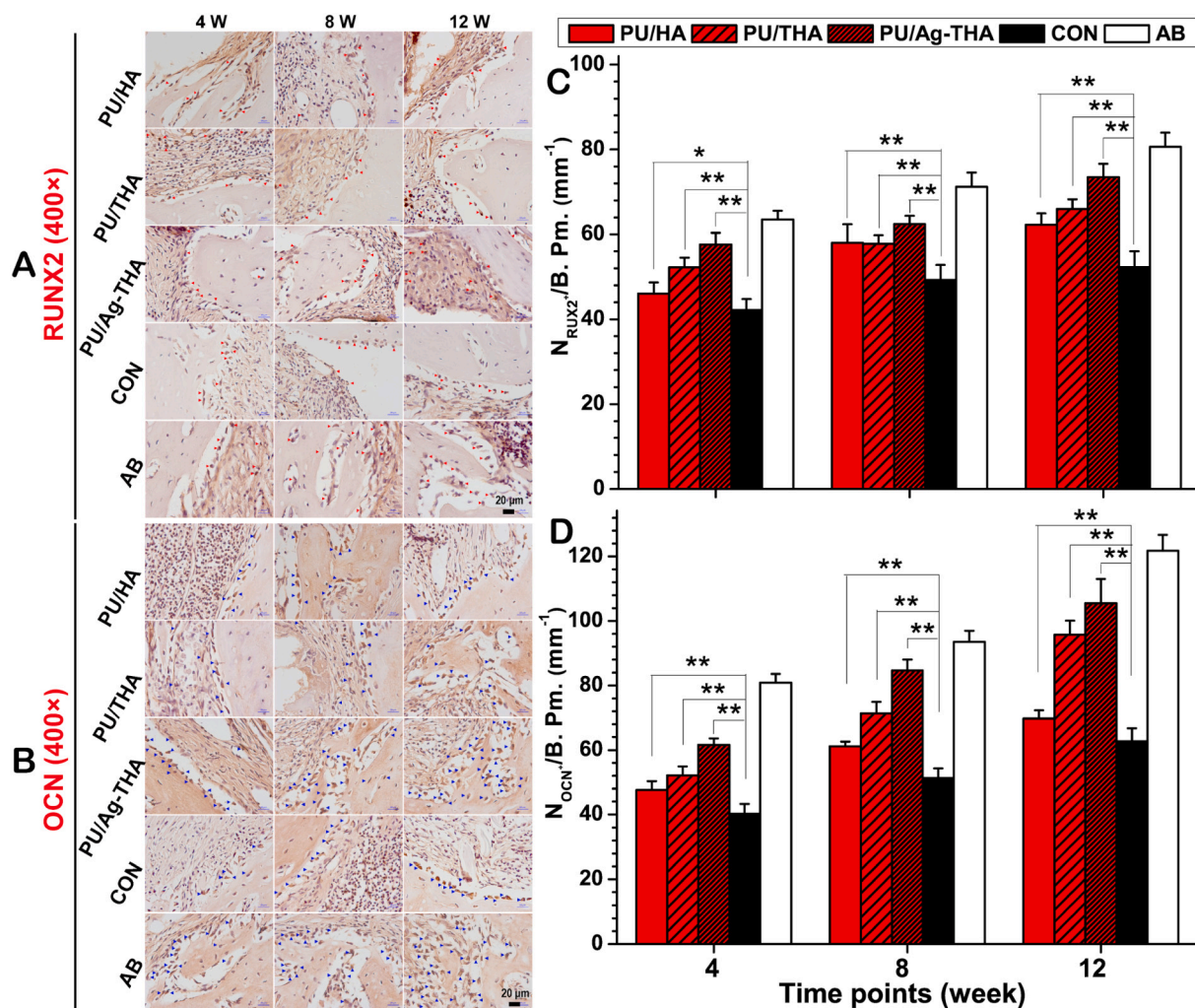


Fig. 6. The immunohistochemical staining images of RUNX2 (Runt-related transcription factor 2, A) and OCN (osteocalcin, B), and the calculated numbers of RUNX2 (C) and OCN (D) positive staining cells per mm length of bone perimeter (B. Pm.), reflecting the osteogenesis in the treated infective bone defects of femoral condyle. The RUNX2 and OCN positive staining cells are pointed out using red color and blue color arrows respectively in the RUNX2 and OCN staining images. * $p < 0.05$, ** $p < 0.01$. (For interpretation of the references to color in this figure legend, the reader is referred to the web version of this article.)

was still mostly filled up with fibrous tissue, with bacteria colonies being wrapped in. Compared to the PU/HA and CON groups, more new bone formation could be found in PU/THA and PU/Ag-THA groups (Fig. 5A and B). In particular, very few bacteria colonies were observed after 12 weeks, and a gradual increase in bone formation over time was evident in the PU/Ag-THA group. These results indicate that in the case of infected bone treatment, the introduction of antimicrobial activity is essential to promote bone regeneration, probably by inhibiting the bacteria colonization thereby facilitating the host osteogenic cells to migrate into the scaffolds for bone repair. Cartilage was detected in the newly formed tissues in all the five groups (Fig. 5B), revealed by the Safranin O and fast green staining images where cartilage was stained orange and bone tissue appeared green (Fig. 5C). Less cartilage surrounding the implanted AB was evident at week 12 than that of week 8 (Fig. 5C) indicating that cartilage formation might be an inherent early stage for bone formation. More cartilage tissue was observed in PU/Ag-THA group than in PU/HA and PU/THA groups (Fig. 5C), suggesting that PU/Ag-THA might promote infected bone regeneration partly through endochondral ossification.

RUNX2 is required for osteoblastogenesis and terminal chondrocyte maturation [37], thus considered as an indicator for the early stage of endochondral bone formation processes [4,37], while OCN is a characteristic indicator for mature osteoblasts [4,38]. RUNX2 and OCN

immunohistochemical staining can be used to characterize the osteoinductivity of bone implants by observing the number change of osteoprogenitor cells (in the early differentiation stage) and mature osteoblasts respectively. As shown in Fig. 6A and B, RUNX2 and OCN positive cells distributed along the surface of the new bone trabeculae, around the material and in the fibrous tissue. The numbers of RUNX2 and OCN positive cells increased with time (Fig. 6C and D). Although the numbers of RUNX2 or OCN positive cells in composite MP groups were lower than that of the AB group, they were significantly higher than that of the CON group (Fig. 6A and B). This could also be seen in the quantitative analysis results shown in Fig. 6C, suggesting that the composite MPs could enhance the differentiation of osteoprogenitor cells and the activity of osteoblasts, thus promoting the regeneration of infected bone defects (Fig. 6A and B). Moreover, the numbers of RUNX2 or OCN positive cells in the PU/Ag-THA group were markedly higher than that of PU/HA and PU/THA groups (Fig. 6C and D).

The histology results above confirmed the considerable *in vivo* antimicrobial activity and biocompatibility of PU/Ag-THA and Ag-THA, together with the favourable osteoconductivity and osteoinductivity of PU/Ag-THA to promote osteogenesis in the infected femoral condyle defect model.

4. Conclusions

Postoperative infections and poor osteogenesis remain to be the two major causes for orthopedic failure. In the present study, the *in vivo* anti-infective activity of tannin mediated silver nanoparticles (NPs)-coated hydroxyapatite (HA) (Ag-THA) and its composites with polyurethane was investigated in an infected femoral condyle defect model on rats. Micro-CT and histological studies revealed the outstanding *in vivo* antimicrobial activity of Ag-THA and PU/Ag-THA. Of note, benefiting from its antimicrobial activity, PU/Ag-THA exhibited markedly improved bone regeneration efficacy in the infected bone regeneration, comparing to its non- or weak- antimicrobial counterparts, which may favor bacteria adherence and colonization, thereby hindering the adherence of host osteogenic cells. RUNX2 and OCN immunohistochemical staining further confirmed the enhanced osteoinductivity of PU/Ag-THA relative to the blank and composite controls. This study further supports the necessity and significance of the use of antimicrobial implants in infected bone regeneration scenarios. Considering the facile one-step and scalable synthesis manner of Ag-THA and its potent antimicrobial capabilities, the present study may provide a new and universal approach for the development of antimicrobial implants by compositing Ag-THA with existing polymeric orthopedic materials to address the challenges in orthopedic surgeries.

CRedit authorship contribution statement

Xingui Tian: Animal study investigation, Data curation, Software; **Zhihui Lu:** Material synthesis, Original draft preparation; **Chying Ma:** Data analysis, Manuscript revision. **Min Wu:** Characterizations, Scheme draft; **Chengfei Zhang:** Professional advice, Manuscript revision; **Yuping Yuan:** Experimental part preparation; **Xiaowei Yuan:** Figure preparation; **Denghui Xie:** Manuscript editing; **Chao Liu:** Co-supervision; **Jinshan Guo:** Supervision, Conceptualization, Methodology, Manuscript revision.

Declaration of competing interest

The authors declare that they have no known competing financial interests or personal relationships that could have appeared to influence the work reported in this paper.

Acknowledgements

The project was supported in part by an Open Research Fund of State Key Laboratory of Polymer Physics and Chemistry, Changchun Institute of Applied Chemistry, Chinese Academy of Sciences, a National Natural Science Foundation of China (NSFC) Grant 81772315, a Natural Science Foundation of Southwest Medical University (2019ZQN105), and Aleo BME, Inc.

References

- [1] P.V. Giannoudis, H. Dinopoulos, E. Tsiridis, *Injury* 36 (Suppl. 3) (2005) S20–S27.
- [2] J. Tang, J. Guo, Z. Li, C. Yang, D. Xie, J. Chen, S. Li, S. Li, G.B. Kim, X. Bai, Z. Zhang, J. Yang, *J. Mater. Chem. B* 3 (2015) 5569–5576.
- [3] Y. Guo, R.T. Tran, D. Xie, D.Y. Nguyen, E. Gerhard, J. Guo, Y. Wang, J. Tang, Z. Zhang, X. Bai, J. Yang, *J. Biomed. Mater. Res. A* 103 (2015) 772–781.
- [4] C. Ma, X. Tian, J.P. Kim, D. Xie, X. Ao, D. Shan, Q. Lin, M.R. Hudock, X. Bai, J. Yang, *Proc. Natl. Acad. Sci. U. S. A.* 115 (2018) E11741–E11750.
- [5] D. Xie, J. Guo, M. Mehdizadeh, R. Tran, R. Chen, D. Sun, G. Qian, D. Jin, X. Bai, J. Yang, *J. Mater. Chem. B* 3 (2015) 387–398.
- [6] J. Guo, Z. Xie, R.T. Tran, D. Xie, D. Jin, X. Bai, J. Yang, *Adv. Mater.* 26 (2014) 1906–1911.
- [7] D. Sun, Y. Chen, R.T. Tran, S. Xu, D. Xie, C. Jia, Y. Wang, Y. Guo, J. Guo, Z. Zhang, J. Yang, D. Jin, X. Bai, *Sci. Rep.* 4 (2014) 6912.
- [8] H. Winkler, P. Haiden, *J. Bone Joint Infection* 2 (2017) 52–62.
- [9] W. Ahmed, Z. Zhai, C. Gao, *Mater. Today Bio* 2 (2019) 100017.
- [10] T. Zhu, Y. Cui, M. Zhang, D. Zhao, G. Liu, J. Ding, *Bioact. Mater.* 5 (2020) 584–601.
- [11] E.L. Cyphert, G.D. Learn, S.K. Hurley, C. Lu, H.A. von Recum, *Adv. Healthc. Mater.* 7 (2018), 1800812.
- [12] R. Dorati, A. DeTrizio, T. Modena, B. Conti, F. Benazzo, G. Gastaldi, I. Genta, *Pharmaceuticals* 10 (2017) 96.
- [13] H.-y. Li, D.-n. Huang, K.-f. Ren, J. Ji, *Smart Mater. Med.* (2020), <https://doi.org/10.1016/j.smaim.2020.10.002>.
- [14] J. Guo, X. Tian, D. Xie, K. Rahn, E. Gerhard, M.L. Kuzma, D. Zhou, C. Dong, X. Bai, Z. Lu, Z.J. Yang, *Adv. Funct. Mater.* 30 (2020) 2002438.
- [15] J. Guo, W. Sun, J.P. Kim, X. Lu, Q. Li, M. Lin, O. Mrowczynski, E. Rizk, J. Cheng, G. Qian, J. Yang, *Acta Biomater.* 72 (2018) 35–44.
- [16] E. Watson, A.M. Tatara, D.P. Kontoyiannis, A.G. Mikos, *ACS Biomater. Sci. Eng.* 3 (2017) 1207–1220.
- [17] J. Guo, W. Wang, J. Hu, D. Xie, E. Gerhard, M. Nisic, D. Shan, G. Qian, S. Zheng, J. Yang, *Biomaterials* 85 (2016) 204–217.
- [18] L.-C. Su, Z. Xie, Y. Zhang, K.T. Nguyen, J. Yang, *Front. Bioeng. Biotechnol.* 2 (2014), <https://doi.org/10.3389/fbioe.2014.00023>.
- [19] J. Guo, G.B. Kim, D. Shan, J.P. Kim, J. Hu, W. Wang, F.G. Hamad, G. Qian, E. B. Rizk, J. Yang, *Biomaterials* 112 (2017) 275–286.
- [20] X. Lu, S. Shi, H. Li, E. Gerhard, Z. Lu, X. Tan, W. Li, K.M. Rahn, D. Xie, G. Xu, F. Zou, X. Bai, J. Guo, J. Yang, *Biomaterials* 232 (2020) 119719.
- [21] W. Wang, K.W.K. Yeung, *Bioact. Mater.* 2 (2017) 224–247.
- [22] C. Wang, P. Makvandi, E.N. Zare, F.R. Tay, L. Niu, *Adv. Therap.* 3 (2020) 2000024.
- [23] J. Raphael, M. Holodniy, S.B. Goodman, S.C. Heilshorn, *Biomaterials* 84 (2016) 301–314.
- [24] M. Cloutier, D. Mantovani, F. Rosei, *Trends Biotechnol.* 33 (2015) 637–652.
- [25] S. Irvani, R.S. Varma, *Green Chem.* 21 (2019) 4583–4603.
- [26] J. Harde, H. Ahrens, C. Gebert, A. Streitberger, H. Buerger, M. Erren, A. Günsel, C. Wedemeyer, G. Saxler, W. Winkelmann, G. Gosheger, *Biomaterials* 28 (2007) 2869–2875.
- [27] S.P. Hudson, R. Langer, G.R. Fink, D.S. Kohane, *Biomaterials* 31 (2010) 1444–1452.
- [28] C. Xie, X. Wang, H. He, Y. Ding, X. Lu, *Adv. Funct. Mater.* 30 (2020) 1909954.
- [29] T.S. Sileika, R. Zhang, D.G. Barrett, P.B. Messersmith, *Angew. Chem. Int. Ed.* 52 (2013) 10766–10770.
- [30] C. Ma, M.L. Kuzma, X. Bai, J. Yang, *Adv. Sci.* 6 (2019), 1900819.
- [31] C. Ma, E. Gerhard, Q. Lin, S. Xia, A.D. Armstrong, J. Yang, *Bioact. Mater.* 3 (2018) 19–27.
- [32] C. Ma, E. Gerhard, D. Lu, J. Yang, *Biomaterials* 178 (2018) 383–400.
- [33] Y. Niu, K.C. Chen, T. He, S. Huang, K. Xu, *Biomaterials* 35 (2014) 4266–4277.
- [34] Y. Niu, L. Li, K.C. Chen, F. Chen, X. Liu, J. Ye, W. Li, K. Xu, *J. Biomed. Mater. Res. Part A* 103A (2015) 2355–2364.
- [35] L. Li, X. Liu, Y. Niu, J. Ye, S. Huang, C. Liu, K. Xu, *J. Biomed. Mater. Res. Part B* 105B (2017) 1200–1209.
- [36] C.T. Johnson, M.C.P. Sok, K.E. Martin, P.P. Kalelkar, J.D. Caplin, E.A. Botchwey, A. J. Garcia, *Sci. Adv.* 5 (2019), eaaw1228.
- [37] M.E. McGee-Lawrence, L.R. Carpio, E.W. Bradley, A. Dudakovic, J.B. Lian, A.J. van Wijnen, S. Kakar, W. Hsu, J.J. Westendorf, *Bone* 66 (2014) 277–286.
- [38] S.C. Moser, B.C.J. van der Eerden, *Front. Endocrinol.* 9 (2019) 794.